J Appl Electrochem (2012) 42:483–490
DOI 10.1007/s10800-012-0423-3

ORIGINAL PAPER

Au/C catalyst prepared by polyvinyl alcohol protection method for direct alcohol alkaline exchange membrane fuel cell application

S. Yongprapat · A. Therdthianwong · S. Therdthianwong

Received: 9 March 2012 / Accepted: 23 April 2012 / Published online: 5 May 2012

Abstract An Au/C catalyst was prepared by means of the polyvinyl alcohol-protected Au sol method. Highly dispersed Au nanoparticles with an average particle size of around 3.7 nm were obtained as confirmed by transmission electron microscopy. The cyclic voltammogram of Au/C was similar to that of a bulk Au electrode, but a small shift of Au oxide reduction and oxidation potential peaks were observed. The electrooxidation of methanol, ethanol, ethylene glycol, and glycerol on the Au/C catalyst in an alkaline solution was analyzed. Using a cyclic voltammogram, the maximum current density toward alcohol electrooxidation was found to decrease in the order of glycerol > ethylene glycol > ethanol, while methanol was not oxidized. Compared with PtRu/C, the maximum current densities obtained from the Au/C catalyst for ethylene glycol and glycerol electrooxidation were increased by 1.6 and 3.3 times, respectively. The reaction heavily progressed through a C–C bond dissociation path. It was found that main product of glycerol electrooxidation was formic acid, which accounted for more than 60 % of the total product. Using chronoamperometry, the Au/C catalyst showed much better stability than that of PtRu/C for the reaction without C–C bond dissociation and better stability for the reaction with C–C bond dissociation.

Keywords Au/C · PVA protection method · Alcohol electrooxidation · Ethanol · Ethylene glycol · Glycerol

S. Yongprapat
Energy Division, Joint Graduate School of Energy and Environment (JGSEE), King Mongkut's University of Technology Thonburi (KMUTT), 126 Pracha-Uthit Road, Bang Mod, Thung Khru, Bangkok 10140, Thailand

A. Therdthianwong (✉)
Fuel Cells and Hydrogen Research and Engineering Center, Clean Energy System Group, PDTI, King Mongkut's University of Technology Thonburi (KMUTT), 126 Pracha-Uthit Road, Bang Mod, Thung Khru, Bangkok 10140, Thailand
e-mail: apichai.the@kmutt.ac.th

S. Therdthianwong
Department of Chemical Engineering, Faculty of Engineering, King Mongkut's University of Technology Thonburi (KMUTT), 126 Pracha-Uthit Road, Bang Mod, Thung Khru, Bangkok 10140, Thailand

1 Introduction

A direct alcohol fuel cell (DAFC), especially direct methanol and direct ethanol fuel cells (DMFC and DEFC), using a proton exchange membrane (PEM) were extensively investigated. The advantages of this type of fuel cell are its low operational temperature and convenient fuel feeding; hence, it is well suited for portable power applications. However, the main limitation of a DAFC based on PEM is the use of an expensive Pt-based catalyst. Pt is known as the most active metal for both alcohol oxidation and oxygen reduction reactions (ORRs) in an acidic environment [1, 2], but the main drawback is its strong interaction with CO and the creation of some reaction intermediates.

Unlike acidic PEM fuel cells DAFCs, alkaline DAFCs allow for the replacement of Pt with less expensive metals, since the electrode reaction in an alkaline cell proceeds differently from that in acidic environments. The alcohol electrooxidation in an alkaline solution can be promoted by many metals, such as Pd [3–5], Au [1, 6, 7], Ag [8, 9], Ni oxide [10, 11], and some Ru alloys [12]. For the ORR, a number of materials are active via four-electron pathways, namely, Pd [13, 14], Ru [15], Au(100) [16], Ag [17–19], Co_3O_4 [20], and MnO_2 [21]. The results indicate that bulk

Au gives a higher current density than Pt for high molecular weight alcohol in alkaline. Moreover, owing to the lack of adsorptive behavior, Au becomes poisoned much less by oxidation intermediates [1].

The studies of alcohol electrooxidation of gold catalysts in alkaline solutions have been conducted on two different forms: bulk gold and supported gold (Au/C). Much of this research was performed with single and polycrystalline gold electrodes, i.e., with monohydric alcohols (methanol and ethanol) [8, 9, 22, 23] or with polyhydric alcohols [6, 24, 25]. The electrocatalytic oxidation on bulk Au is affected by surface crystallography depending on the reactant's structure. On the other hand, there have been only a few investigations conducted into the supported Au/C performance on alcohol electrooxidation [13, 26]. The carbon-supported Au catalyst has been tested for oxygen electroreduction in alkaline electrolytes by many research groups [27–31] and its activity is size dependent.

Recently, for DMFCs, unsupported Pt black is being replaced with supported Pt/C catalysts to maximize active surface area in an effort to reduce anode Pt loading [32]. In this study, the high loading Au/C (20 wt% Au) catalysts prepared by polyvinyl alcohol (PVA) protection method were tested for their catalytic activities toward the electrooxidation of ethanol, ethylene glycol, and glycerol. Furthermore, the possibility of utilizing the Au/C catalysts in fuel cell applications was evaluated by conducting a stability test of the catalyst using chronoamperometry technique. The products from the reaction were analyzed by means of prolonged electrolysis to explore the possible causes of Au/C instability. Finally, the performance of the Au/C catalysts was compared to that of a commercial PtRu/C catalyst.

2 Experimental procedure

2.1 Catalyst preparation

The gold sol was first prepared using PVA as a protecting agent. The aqueous solution of an Au precursor ($HAuCl_4{\cdot}3H_2O$, Aldrich, 99.9 %) at an Au concentration of 110 μg ml^{-1} was mixed with 1 wt% PVA solution (Fluka, MW ~22,000). A 0.1 M $NaBH_4$ solution (APS, 97 %) was added dropwise at the Au:$NaBH_4$ ratio of 1:4 under vigorous stirring to obtain a ruby red Au sol. After full formation, the well-dispersed Vulcan XC-72R (Cabot Corporation) in ethanol (Carlo Erba, 99.8 %) was added to the sol to immobilize the Au nanoparticles under stirring for 3 h. The complete adsorption of Au nanoparticles on carbon was observed from the disappearance of the color of the solution, as well as confirmed later by atomic absorption spectroscopy (AAS) measurements. The catalyst mixture was then filtered and washed by ethanol and deionized water (with Cl^- test). Finally, the catalyst was dried in a vacuum oven at 70 °C for 30 min.

2.2 Catalyst characterization

Transmission electron microscopy (TEM) images of the catalysts were captured from JEOL JEM-2010 at 200 keV. The sizes of the Au nanoparticles were measured from the TEM images at a magnification of 100,000 times for at least 500 particles. The mean particle diameter (d_m) was calculated by means of the formula:

$$d_m = \sum d_i n_i / \sum n_i \quad (1)$$

where n_i is the number of particles having the diameter d_i.

The size of the Au nanoparticles in the Au sol was also roughly estimated by visible UV. The maximum absorption wavelength (λ_{max}) of the freshly prepared gold sol was measured using Genesys 10 series UV spectrophotometer of Thermo Scientific.

For electrochemical measurements, the working electrode was prepared by dropping the catalyst ink onto a glassy carbon electrode (Bas Inc.). The catalyst ink was composed of a certain amount of catalyst and 5 wt% Nafion solution (Dupont) in isopropanol (QRëC, 99.7 %). The ink was made homogenous by ultrasonic mixing for at least 30 min. This well-mixed ink was dropped onto a well-polished glassy carbon to prepare a working electrode using a micropipette under hot air to yield a catalyst loading of 200 μg cm^{-2}. Mercury/mercury oxide (1.0 M NaOH) was used as the reference electrode. Two types of counter electrode were employed: 1 cm^2 Au gauze (Alfa Aesar, 52 mesh woven from 0.102-mm diameter wire) for voltammetric and chronoamperometric (CA) study and glassy carbon electrode for the electrolysis measurement. The electrolyte was degassed by flowing Ar gas (TIG, high purity) for at least 30 min before use. The bulk gold electrode used for comparison was 1.45-cm gold wire of 1.0-mm diameter (Premion®, 99.999 %).

The cyclic voltammetry and chronoamperometry measurements were conducted using SI1287 potentiostat (Solartron). The catalytic properties of the catalysts toward four types of alcohol, including methanol (Merck, 99.9 %), ethanol, ethylene glycol (Sigma Aldrich, 99.0 %), and glycerol (Ajax, 99.5 %), were studied.

The stability of the catalyst was resolved by the long-term poisoning rate (δ) from CA results. The long-term poisoning rate was computed using the steady decay rate of potentiostatic curves (dI/dt) according to the following relationship [33]:

$$\delta = (100/I_0) \times (dI/dt) \quad (2)$$

where δ is the long-term poisoning rate (% per s), I_0 is the current at the start of polarization extrapolated back from the linear current decay, and $(dI/dt)_{t>600}$ is the average slope of the curve from 600th to 3,000th s.

To calculate the average slope of the CA curve, the linear range of the CA curve was used. Therefore, the time interval used in this study was extended from 500th to 600th s.

The prolonged electrolysis was carried out using Autolab PGSTAT 302 N. The electrolysis program was written by a NOVA program, consisting of three main steps: 1 min for electrolysis at a specified potential, and two short clean potentials at 1.2 and 0.8 V for 0.1 and 0.2 s, respectively.

The prolonged electrolysis products were analyzed by high performance chromatography (Prominence HPLC, Shimadzu) equipped with a refractive index detector (RID10A). Column KC-811 (Shodex) was used along with 0.1 % H_3PO_4 (QRëC, 85 %) as a mobile phase. The list of standard reagents were formic acid (QRëC, 85 %), glycolic acid (Fluka, 97 %), oxalic acid (Riedel de Haën, 99.5 %), glyceric acid (Alfa Aeser), and tartronic acid (Fluka, 97 %).

3 Results and discussions

3.1 Physical characterization

Figures 1 and 2 show the TEM images of 10 % Au/C and 20 % Au/C at the magnification of ×100,000, respectively. The Au was observed as nanosize particles (black dot) on the larger carbon support (gray area). The Au particles were well dispersed in both catalysts. Most of the particles were deposited uniformly on the carbon surface without cluster formation. The majority of Au nanoparticles in both catalysts had a size of 3.5 nm with a very narrow size distribution, as illustrated in Fig. 3. Around 95 % of particles were in the size range of 3.00–5.00 nm. The average sizes of 10 and 20 % Au/C were 3.69 ± 0.56 and 3.81 ± 0.64 nm, respectively. The size of the synthesized catalyst was slightly larger than that of a commercial PtRu/C reported at 3.2 nm [34].

The electron diffraction pattern of 20 % Au/C in Fig. 4 indicates the Au nanoparticles with pure Au. The nanoparticle was polycrystalline Au with an fcc crystal. The reflecting planes of {111}, {200}, {220}, and {311} were visualized.

The size of the Au nanoparticles can be roughly estimated by means of the UV–Visible technique as published by Porta et al. [35]. In comparison with the λ_{max} in their study, the measured λ_{max} of 505 nm should yield Au particles with a size of around 3–4 nm. This value was in concurrence with the TEM results. Despite a much higher loading of Au in this study, a similar Au particle size was obtained for both the 20 wt% Au/C prepared in this study and the 1 wt% Au/C prepared by Porta et al., indicating that the size of Au particles had not been altered in the immobilization step.

The TEM results show a similar morphology in both prepared catalysts in terms of excellent Au dispersion with narrow size distribution. Hence, Au loading of 20 wt% was

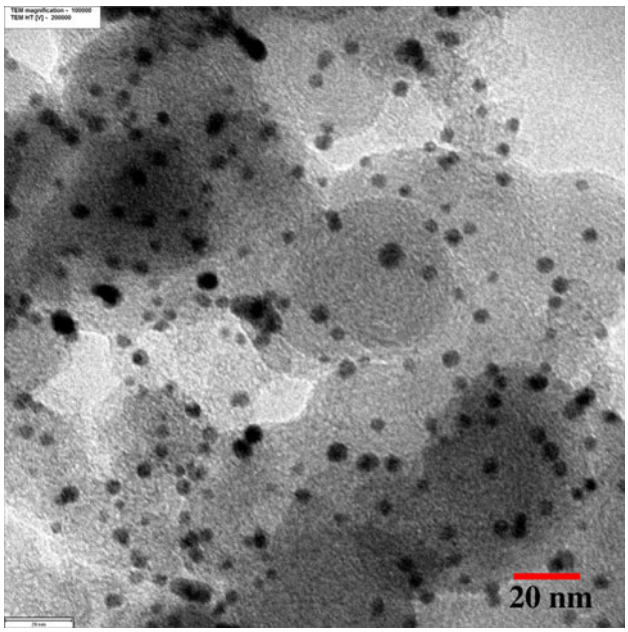

Fig. 1 TEM image of 10 % Au/C at magnification of ×100,000

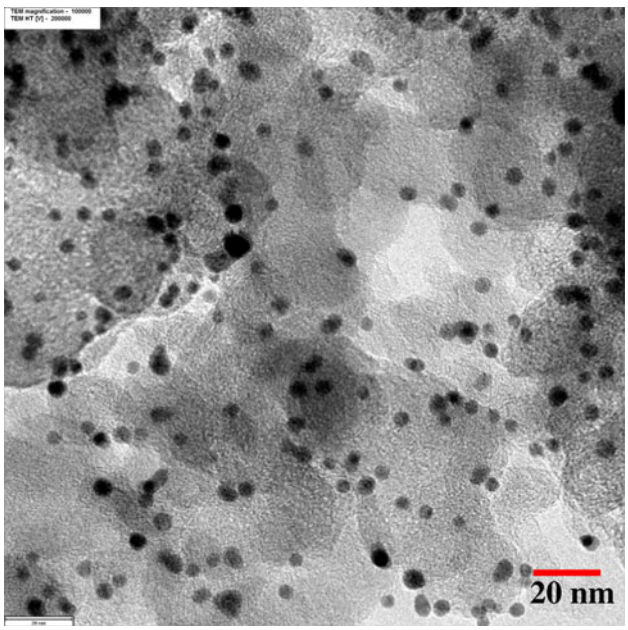

Fig. 2 TEM image of 20 % Au/C at magnification of ×100,000

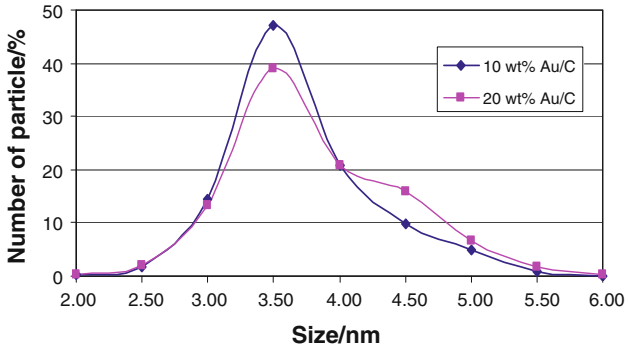

Fig. 3 Histogram of size distribution of Au nanoparticle on 10 and 20 % Au/C catalysts

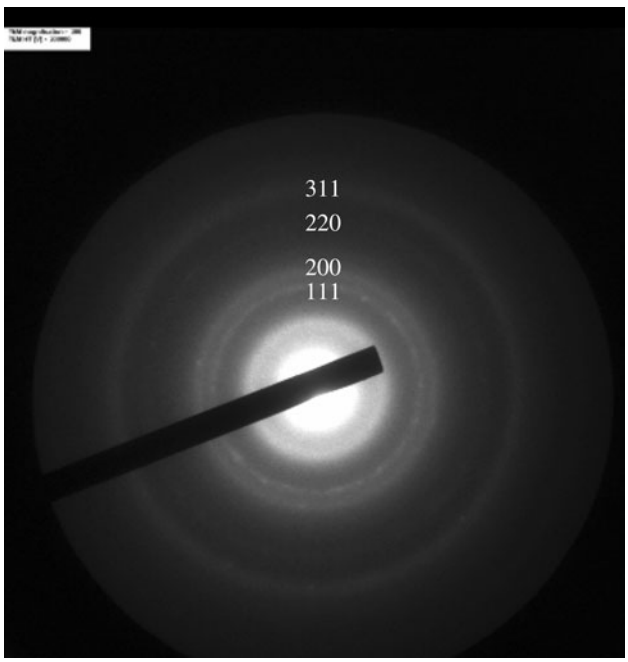

Fig. 4 Electron diffraction ring pattern of 20 % Au/C catalyst

used for the remaining study to minimize the thickness of the catalyst layer in the fuel cell electrode.

3.2 Electrochemical characterization

The CVs of 20 % Au/C and bulk Au electrodes are comparable as displayed in Fig. 5. Both electrodes exhibited two oxide reduction peaks and small oxidation peaks. A surface oxide film was formed during the positive scan and subsequently reduced in the negative sweep. These two reduction peaks correspond to two distinct oxide layers within the oxide film [36]. The first reduction peak at around 0.2 V and the second peak at 0.0 V are the reductions of quasi-2D and quasi-3D oxide states, respectively.

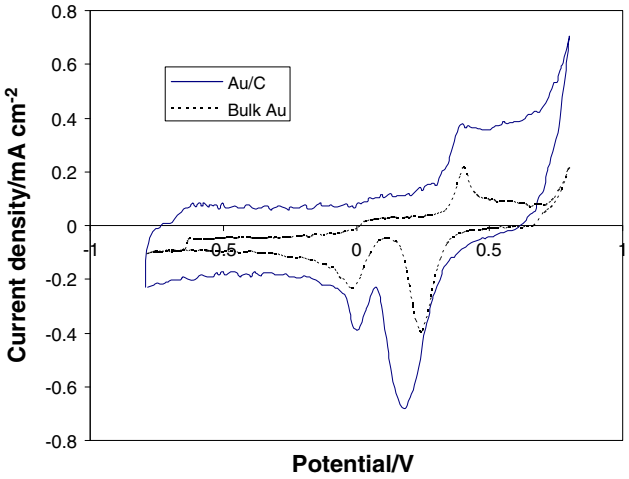

Fig. 5 CVs of 20 % Au/C and bulk Au in 0.1 M KOH at scan rate of 20 mV s^{-1}

For the Au/C electrode, a large double layer charging according to the presence of carbon (~0.0 V Vs. Hg/HgO electrode) was noticed. It should also be mentioned that the oxide reduction peak of the Au/C electrode appeared at a slightly lower potential than that of the bulk Au electrode (i.e., the first reduction peak of the Au/C and of the bulk Au electrodes occurred at 0.2 and 0.25 V, respectively). This negative shift of the reduction potential in the Au/C electrode might have been caused by the particle size effect. By applying the value of an accepting charge of 0.386 mC for 1 cm^2 of gold [36] with the charge density under the quasi-2D oxide reduction peak, the ESA of 5.95 m^2 g^{-1} was obtained.

3.3 Alcohol electrooxidation

Figure 6 shows the CV of the alcohol electrooxidation on 20 % Au/C. There were three oxidizable alcohols on Au/C, which were ethanol, ethylene glycol, and glycerol. All the alcohol oxidation began at around the same potential region after the adsorption of hydroxide on the surface of the Au as shown the $onset_F$ in Table 1. The current density increased with increasing potential and reached the maximum at around 0.4 V. At this potential, the film of oxide formed on the surface of the Au and prevented further alcohol electrooxidation. Hence, the current density decreased and reached the background current. In the reverse scan, the alcohol oxidation was inhibited by the oxide film. After the oxide reduction had taken place, the alcohol electrooxidation ability of the Au was recovered. The electrooxidation activities of the Au for ethylene glycol and glycerol in the reverse scan were nearly the same as that in the forward scan for the same potential region (See the I_F/I_R ratio in Table 1). This indicated excellent reversibility for the Au catalyst.

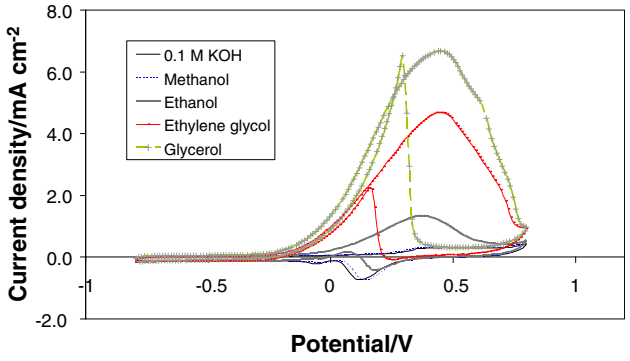

Fig. 6 CVs of 20 %Au/C in 0.1 M KOH with 0.1 M of its respective alcohols at scan rate of 20 mV s^{-1}

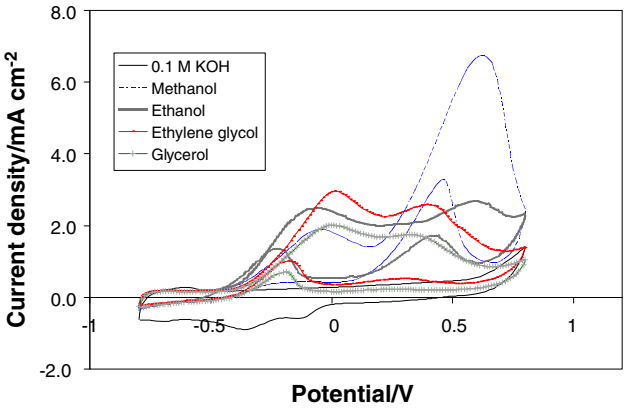

Fig. 7 CVs of 20 % PtRu/C in 0.1 M KOH with 0.1 M of its respective alcohols at scan rate of 20 mV s^{-1}

It was found that the alcohol with the highest activity in this study was glycerol, followed by ethylene glycol and ethanol, while the methanol had not oxidized, because the oxidation reaction of adsorbed alcohol was very fast, and the overall alcohol electrooxidation rate was controlled by the adsorption step. The adsorption of alcohol on the Au surface can be in the form of alkoxide adsorption, controlled by pK_a, [37] or dissociative adsorption of β-H induced by the preadsorbed hydroxide on the Au surface, controlled by van der Waals' force [1].

For comparison, the electrooxidation of alcohols on PtRu/C was conducted at the same conditions, as shown in Fig. 7. The reaction of all alcohols took place in two potential regions. Table 2 shows the characteristics of the main oxidation peaks. The activity of alcohol oxidation on PtRu was in the reverse order with that of Au. The most active alcohol reacting on PtRu was methanol, followed by ethylene glycol, ethanol, and glycerol. The rate-determining step on PtRu was the oxidation of the poisoning species on the surface. The reaction rate on the PtRu-based catalyst was controlled by the steric effect [1]. A larger molecule covers more area on the Pt surface and prevents a new reacting molecule from reaching the Pt surface.

The alcohol electrooxidation reaction on PtRu/C occurs at a more negative potential than that on Au/C. The onset potential for all alcohols on PtRu/C was around −0.5 V with the maximum peak current at around 0.0 V. In terms of catalytic activity, PtRu/C shows superior activity for methanol and ethanol electrooxidation. For ethylene glycol, Au/C was better in terms of current density, but with more positive peak potential. More importantly, Au/C performed much better than PtRu/C for glycerol electrooxidation with more than a threefold increase in current density. The lower I_f/I_r ratio for ethylene glycol and glycerol on Au/C shows greater reversibility of the active surface over PtRu/C, as confirmed later by CA study.

3.4 Chronoamperometric and prolonged electrolytic study

The CA curves at 0.2 and 0.4 V of ethanol, ethylene glycol, and glycerol electrooxidation on Au/C are shown in Fig. 8. The potential of 0.4 V was selected because the highest activity of the Au/C catalyst was achieved at about this potential. However, rather than letting it be poisoned by the surface intermediate, the reaction on the Au can be halted by the oxide film on its surface. This film was formed at a potential of around 0.4 V; thus, the potential of 0.2 V was selected in conducting chronoamperometry to compare the effects of the oxide formation. The results showed the same trend as that in the cyclic voltammogram. The current density gained followed the descending order of glycerol > ethylene glycol > ethanol. Moreover, the catalytic activity at 0.4 V was higher than that at 0.2 V.

Table 3 shows the calculated long-term decay rate for Au/C in comparison with PtRu/C. The potential used for PtRu/C was the potential at the maximum current density of both peaks, which were at 0.0 and 0.4 V. For the Au/C,

Table 1 The electrocatalytic activity of alcohol electrooxidation on 20 % Au/C

Alcohol	$Onset_F$ (V)	$I_{F_{max}}$ (mA cm^{-2})	$V_{IF_{max}}$ (V)	$Onset_R$ (V)	$I_{R_{max}}$ (mA cm^{-2})	$V_{IR_{max}}$ (V)	I_F/I_R
Ethanol	−0.330	1.348	0.377	0.128	0.196	0.074	6.88
Ethylene glycol	−0.330	4.688	0.449	0.226	2.240	0.158	2.09
Glycerol	−0.360	6.664	0.448	0.453	6.520	0.293	1.02

Table 2 The electrocatalytic activity of alcohol electrooxidation on 20 % PtRu/C

Alcohol	Peak	$Onset_F$ (V)	$I_{F_{max}}$ (mA cm^{-2})	$V_{IF_{max}}$ (V)	$Onset_R$ (V)	$I_{R_{max}}$ (mA cm^{-2})	$V_{IR_{max}}$ (V)	I_F/I_R
Methanol	1st peak	−0.54	1.90	−0.06	–	–	–	–
	2nd peak	0.35	6.73	0.62	0.66	3.31	0.46	2.03
Ethanol	1st peak	−0.58	2.50	−0.06	−0.10	1.36	−0.23	1.83
Ethylene glycol	1st peak	−0.50	2.96	0.01	−0.03	1.01	−0.18	2.94
Glyerol	1st peak	−0.50	2.01	−0.00	−0.10	0.71	−0.19	2.84

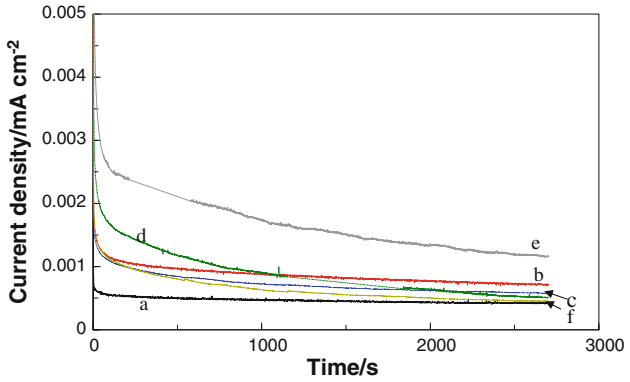

Fig. 8 The chronoamperometric curves for the electrooxidation of ethanol on Au/C catalyst at **a** 0.2 V, **b** 0.4 V, ethylene glycol at **c** 0.2 V, **d** 0.4 V and glycerol at **e** 0.2 V and **f** 0.4 V in 0.1 M KOH and 0.1 M of alcohol

Table 3 The long-term decay rate of alcohol electrooxidation on Au/C and PtRu/C

Alcohol	Potential (V)	Decay rate (δ, % per s)	
		Au/C	PtRu/C
Ethanol	0.0	–	0.0233
	0.2	0.0068	–
	0.4	0.0108	0.0178
Ethylene glycol	0.0	–	0.0213
	0.2	0.0125	–
	0.4	0.0227	0.0207
Glycerol	0.0	–	0.0202
	0.2	0.0171	–
	0.4	0.0185	0.0228

the long-term decay rate in glycerol was the highest followed by ethylene glycol and ethanol, except ethylene glycol at 0.4 V. Moreover, the long-term decay rate at 0.4 V was always higher than that at 0.2 V. A higher long-term decay rate might have resulted from many causes: the formation of the oxide film blocking the Au surface from further reaction, the higher turnover rate, and the difference in reaction pathways.

The products found from the prolonged electrolysis of ethylene glycol and glycerol on Au/C are shown in Table 4. The conversion of both alcohols increased with increasing potential, since more current was generated at 0.4 V. For ethylene glycol, the main electrolysis products were glycolic acid and formic acid. No oxalic acid was found. At a higher operating potential (0.4 V), the formic acid yield was greater than at a low operating potential (0.2 V). This indicates an increase of C–C bond breaking with ethylene glycol by Au/C at higher potential. Consequently, the poisoning rate was also raised at the potential of 0.4 V.

For the glycerol electrolysis on Au/C, a number of products starting from one carbon up to three carbon molecules were yielded. Interestingly, the main product was formic acid with higher than 60 % yield. The other major products were glycolic acid, glyceric acid, and tartronic acid. However, tartonic acid disappeared at a higher potential (0.4 V), while low carbon molecule products increased. This clearly indicated that the dissociative reaction had been favored in glycerol electrooxidation on Au/C and had been enhanced at higher potential.

According to the glycerol electrooxidation mechanism proposed by Kwon et al. [24], as indicated in Fig. 9, there are two different pathways. The first pathway progresses

Table 4 The product distribution in percent for ethylene glycol and glycerol prolonged electrolysis for 20 h

Alcohol	Potential (V)	Conversion (%)	Product (%)				
			Formic acid	Glycolic acid	Oxalic acid	Glyceric acid	Tartronic acid
Ethylene glycol	0.2	4.25	26.32	73.89	n.d.	–	–
	0.4	12.03	36.2	63.8	n.d.	–	–
Glycerol	0.2	9.66	60.39	19.86	2.53	7.58	9.64
	0.4	14.49	67.8	21.74	1.5	8.96	n.d.

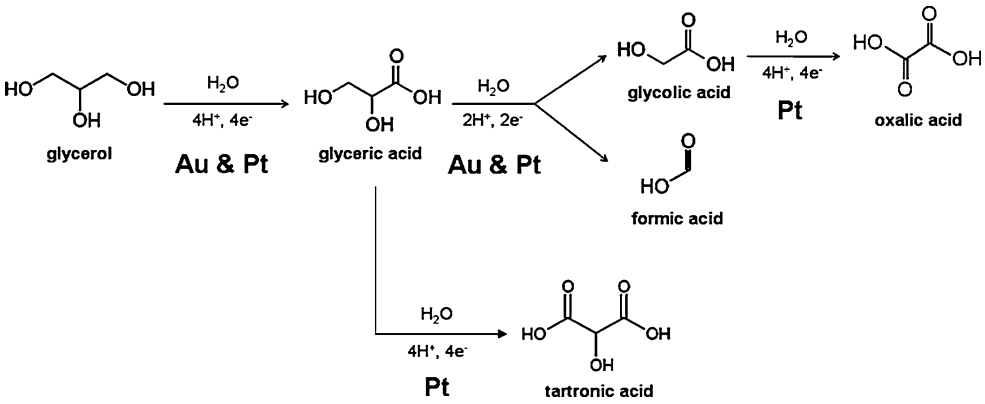

Fig. 9 Reaction pathway for glycerol electrooxidation on Pt and Au [23]

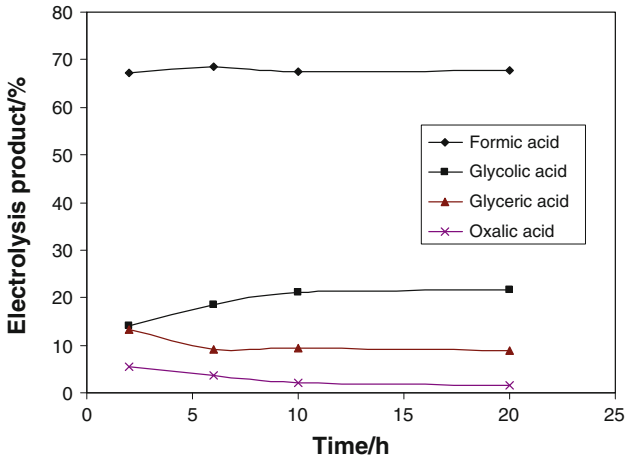

Fig. 10 Product distribution of glycerol electrooxidation on Au/C at 0.4 V

without poisonous intermediates, and the final product is tartronic acid. Another pathway involves the C–C scission that yields formic acid and glycolic acid or oxalic acid as final products.

High formic acid yield suggested that there is a possible reaction pathway generating this product. Formic acid was formed as a primary product since the percentage of formic acid was nearly constant from the beginning, as shown in Fig. 10. The product obtained from glycerol electrooxidation on Au/C at 0.4 V contained about 67 % formic acid. It was also observed that glycolic acid increased with time, while glyceric acid and oxalic acid were slightly reduced with time.

The prolonged electrolysis of ethylene glycol on Au/C also gives formic acid as one of the main products. Thus, formic acid was obtained as a cleavage product from the pre-adsorbed glycolic acid:

$$CH_2OHCOOH + 2OH^- \rightarrow 2HCOOH + H_2O + 2e^- \quad (3)$$

On bulk Au, the above reaction may occur to a very low extent, since formic acid and glycolic acid were formed in equal amounts at all potentials [24]. This unusual catalytic property of Au/C over bulk Au was also observed in other reactions, such as CO oxidation. The main effect attributed to the special catalytic properties of the supported Au/C catalyst was related to the higher availability of low-coordinate Au atoms on the nanoparticles [38]. The higher binding energy between such Au atoms and carbon may activate the dissociation of C–C bonds in glycolic acid and yield formic acid as a final product. The product analysis of ethanol was not performed in this study. However, from the proposed mechanism [23], the reaction on Au did not involve C–C bond dissociation and yielded acetic acid as a final product.

The long-term decay rate data in Table 3 indicates better stability of the Au/C catalyst over the PtRu/C. On the Pt-based catalyst, the scission of the C–C bonds may provide CO molecules that are strongly adsorbed on Pt, and the adsorbed species reduces the activity of the catalyst. The reaction of ethanol on Pt produces CO from adsorbed acetaldehyde by the following equations [39]:

$$Pt + CH_3CHO \rightarrow Pt\text{-}(CO\text{-}CH_3)_{ads} + H^+ + e^- \quad (4)$$

$$Pt + Pt(CO\text{-}CH_3)_{ads} \rightarrow Pt\text{-}(CO)_{ads} + Pt\text{-}(CH_3)_{ads} \quad (5)$$

Ethylene glycol electrooxidation also generates adsorbed CO from the reaction of glycolate to formate, which can be further oxidized to CO [6, 40]. This reaction appears at a more negative potential and with greater quantity on Pt than that on Au [6]. For glycerol electrooxidation, the reaction pathway on Pt was similar to that on Au with higher oxidation degree to oxalic and tartonic acids [24].

With regard to the mechanism above, the stability of the Au/C catalyst was much greater for the reaction with no C–C dissociation as in ethanol electrooxidation or close to that of PtRu/C for the reaction with C–C scission involved, as in ethylene glycol and glycerol electrooxidation. This indicates that the products of the dissociation could have lowered the stability of Au as in Pt-based catalysts, even though poisonous species on Pt, such as CO, were not strongly adsorbed on Au [41].

4 Conclusions

The Au/C catalyst was synthesized from the PVA-protected Au sol. TEM images of Au/C catalyst of two loadings at 10 and 20 wt% Au/C illustrate well-dispersed polycrystalline Au nanoparticles on the carbon support. The average size of the Au particles in both loadings was very close at around 3.7 nm.

The CV of Au/C in alkaline was similar to that of the bulk Au electrode. The Au oxide formation and reduction on both electrodes occurred at around the same potential. The quasi-2D oxide reduction peaks on Au/C shift to a more negative potential because of the particle size effect. The ESA of 5.95 $m^2\ g^{-1}$ of catalyst was obtained for 20 wt% Au/C.

The alcohol electrooxidation of Au/C obeys the general trend of the alcohol electrooxidation on bulk Au electrode. The most oxidizable alcohol was glycerol followed by ethylene glycol and ethanol, while methanol was not oxidized. In comparison to PtRu/C, the Au/C catalyst was more active for ethylene glycol and glycerol electro-oxidation. The maximum currents gained on Au/C were greater by 1.6 and 3.3 times than those on PtRu/C for ethylene glycol and glycerol, respectively.

The electrolysis of ethylene glycol yielded only glycolic acid and formic acid as final products. For glycerol electrooxidation, the reaction was heavily preceded via a C–C cleavage pathway. The main product was formic acid, which contributed more than 60 % of the total product. This was dissimilar to the reaction on bulk Au, which emphasized the particle size effects of the nanosize supported catalyst.

The stability of the Au/C strongly links to the reaction mechanism. The Au/C catalyst was very stable for the reaction with no C–C bond dissociation, such as ethanol electrooxidation. Even for the reaction strongly involving the C–C bond dissociation, such as glycerol electro-oxidation, the stability of Au/C was better than that of the PtRu/C catalyst.

Acknowledgments The financial supports for this research from the National Nanotechnology Center of Thailand (NANOTEC), and the Joint Graduate School of Energy and Environment (JGSEE) are greatly appreciated. The first author would like to thank the Thailand Research Fund (TRF) for the Royal Golden Jubilee (RGJ) scholarship.

References

1. Betowska-brzezinska M, Uczak T, Holze R (1997) J Appl Electrochem 27:999
2. Lamy C, Belgsir EM, Léger JM (2001) J Appl Electrochem 31:799
3. Yougui C, Lin Z, Juntao L (2007) Chin J Catal 28(10):870
4. Shen PK, Xu C (2006) Electrochem Commun 8:184
5. Pattabiraman R (1997) Appl Catal 153:9–20
6. Change S, Ho Y, Weaver MJ (1991) J Am Chem Soc 113:9506
7. Zhang JH, Liang YJ, Li N, Li ZY, Xu CW, Jiang SP (2012) Electrochim Acta 59:156–159
8. Avramov-Ivić M, Jovanović V, Vlajnić G, Popić J (1997) J Electroanal Chem 423:119
9. Avramov-Ivić M, Štrbac S, Mitrović V (2001) Electrochim Acta 46:3175
10. Weng Y, Chou T (2003) J Electrochem Soc 150(6):C385
11. Kim J, Park S (2003) J Electrochem Soc 150(11):E560
12. Tarasevich MR, Karichev ZR, Bogdanovskaya VA, Kapustin AV, Lubnin EN, Osina MA (2005) Russ J Electrochem 41(7):829
13. Bunazawa H, Yamazaki Y (2009) J Power Sour 190:210
14. Yang Y, Zhou Y, Cha C (1995) Electrochim Acta 40(16):2579
15. Prakash J, Joachin H (2000) Electrochim Acta 45:2289
16. Shao MH, Adzic RR (2005) J Phys Chem B 109:16563
17. Blizanac BB, Ross PN, Markovic NM (2007) Electrochim Acta 52:2264
18. Demarconnay L, Contauceau C, Léger JM (2004) Electrochim Acta 49:4513
19. Varcoe JR, Slade RCT, Wright GL, Chen Y (2006) J Phys Chem B 110:21041
20. Ling NH, Prestat M, Gautier JL, Koenig JF, Poillerat G, Chartier P (1996) Electrochim Acta 42(2):197
21. Lima FHB, Calegaro ML, Ticianelli EA (2006) J Electroanal Chem 590:152
22. Borkowska Z, Tymosiak-Zielinska A, Shul G (2004) Electrochim Acta 49:1209
23. Tremiliosi-Filho G, Gonzalez ER, Motheo AJ, Belgsir EM, Léger JM, Lamy C (1998) J Electroanal Chem 444:31
24. Kwon Y, Koper MTM (2010) Anal Chem 82(13):5420
25. Hamelin A, Ho Y, Chang S, Gao X, Weaver MJ (1992) Langmuir 8:975
26. Simões M, Barenton S, Contanceau C (2010) Appl Catal B Environ 93:354
27. Chen W, Tang Y, Bao J, Gao Y, Liu C, Xing W, Lu T (2007) J Power Sour 167:315
28. Inasaki T, Kobayashi S (2009) Electrochim Acta 54:4893
29. Shao MH, Adzic RR (2005) J Phys Chem B Lett 109:16563
30. Tang W, Lin H, Kleiman-Shwarsctein A, Stucky GD, McFarland EW (2008) J Phys Chem C 112:10515
31. El-Deab M, Ohsaka T (2002) Electrochim Acta 47:4255
32. Hui R, Fergus J, Li X (2010) Proton exchange membrane fuel cells: materials properties and performance. CRC Press, New York
33. Guo JW, Zhao TS, Prabhuram J, Chen R, Wong CW (2006) J Power Sour 156:345
34. Wongyao N, Therdthianwong A, Therdthianwong S (2010) Fuel 89:971
35. Porta F, Prati L, Rossi M, Scari G (2002) J Catal 211:464
36. Tremiliosi-Filho G, Dall'Antonia LH, Jerkiewicz G (1996) J Electroanal Chem 422:149
37. Kwon Y, Lai SCS, Rodriquez P, Koper MTM (2011) J Am Chem Soc 133:6914
38. Lopez N, Jbanssens TVW, Clausen BS, Xu Y, Mavrikakis M, Bligard T, Nørskov JK (2004) J Catal 223:232
39. Lamy C, Lima A, LeRhun V, Delime F, Coutanceau, Léger JM (2002) J Power Sour 105:283
40. Matsuoka K, Iriyama Y, Abe T, Matsuoka M, Ogumi Z (2005) Electrochim Acta 51:1085
41. Abild-Pedersen F, Andersson MP (2007) Surf Sci 601:1747